Computers and Geotechnics 39 (2012) 116–123

Contents lists available at SciVerse ScienceDirect

Computers and Geotechnics

journal homepage: www.elsevier.com/locate/compgeo

Numerical modeling of traffic-induced ground vibration

Mohannad Mhanna, Marwan Sadek *, Isam Shahrour

Laboratory of Civil Engineering and geoEnvironment (LGCgE), University of Lille 1-Polytech-Lille, Villeneuve d'Ascq 59655, France

ARTICLE INFO

Article history:
Received 15 January 2011
Received in revised form 9 July 2011
Accepted 13 July 2011
Available online 18 November 2011

Keywords:
Traffic
Vehicle
Vibration
Numerical model
Road unevenness

ABSTRACT

Ground vibrations due to road traffic constitute a major environmental problem. This paper presents a numerical model for the analysis and prediction of the ground vibrations due to the road traffic. A car model with four degrees of freedom is used for the determination of the load due to the road traffic. The load is then introduced in a 3D finite difference model for the determination of the traffic-induced ground vibrations. The numerical model is validated using field data. Numerical analyses show that both the amplitude and frequency of the traffic-induced vibrations are mainly affected by the vehicle speed, the road unevenness and the vehicle suspension system. Some recommendations are suggested for the reduction of these vibrations.

1. Introduction

Traffic-induced vibrations can cause discomfort to residents, perturbation of sensitive equipment and even damage to nearby structures. Over the past several years, experimental studies have analyzed the ground vibrations generated by vehicles. Experiments performed at the Transport and Road Research Laboratory [1,2] showed that heavy vehicles mainly caused the perceptible vibrations and that the level of vibrations increased with the vehicle speed and the height and depth of pavement surface irregularity. Crispino and D'Apuzzo [3] conducted a series of measurements of road traffic-induced vibrations in a heritage building in Naples; they used a modified Watts' formula for the determination of the vibration variation with the vehicle type and speed. Other experimental works attempted to correlate the vibration characteristics (level and frequency content) to the bus suspension system [4] and the seasonal climate variation [5].

Theoretical and numerical studies have also been conducted. Lombaert and Degrande [6,7] used the boundary element method in the frequency–wave number domain together with the Betti-Rayleigh reciprocal theorem to compute the dynamic response induced by a moving vibration source. Their model was validated using field tests. D'Apuzzo [8] reported that, when the road roughness was described through a singular surface unevenness, the stationarity of the excitation was not satisfied and that the transitional feature of the dynamic vertical forces must be properly described. Shen [9] proposed a finite element model to investigate the characteristics of the building vibrations induced by adjacent moving truck crossing random irregularities. He indicated that the coincidence of the natural vertical frequency of the truck and the first natural frequency of the building should be avoided. The stochastic approach was also used by Xu and Hong [10] to quantify the traffic-induced building vibrations; they showed that traffic-induced ground vibrations disrupted high-tech facilities.

The vibration level and frequency depend on several factors such as vehicle weight and speed, suspension system, road condition and soil characteristics. Based on the Betti–Rayleigh Dynamic Reciprocal Theorem and the reciprocal property of the Green's functions, Cao et al. [11] developed a Matlab code for the determination of the ground to moving and harmonic loads. They reported that the ground vibration induced by moving loads is a typical low-frequency problem controlled by the Rayleigh wave in the top soil layer. Hajek et al. [12] reported that the pavement surface irregularity caused loads characterized by a body bounce movement (0.8–4 Hz) and an axle hop movement (8–15 Hz).

Beskou and Theodorakopoulos [13] have recently provided a comprehensive review on the dynamic response of pavements to moving loads and they have stressed the need of the need of field data for the development and calibration of numerical models.

This paper presents a global numerical model for the analysis in the time-domain of the traffic-induced vibrations. The numerical modeling is conducted in two stages. In the first stage, a car model with four degrees of freedom is used for the determination in the time domain of the load due to road irregularities. In the second stage, a 3D finite difference model using the FLAC 3D program is used to determine the ground vibrations due to the load determined in the first stage.

* Corresponding author.
E-mail addresses: mohannad.mhanna@polytech-lille.net (M. Mhanna), marwan.sadek@polytech-lille.fr (M. Sadek), isam.shahrour@univ-lille.fr (I. Shahrour).

0266-352X/$ - see front matter © 2011 Elsevier Ltd. All rights reserved.
doi:10.1016/j.compgeo.2011.07.005

The originality of the paper relies on the use of a global numerical model for the prediction of the traffic-induced ground vibrations, with realistic modeling of both the load due to the road traffic and the ground vibrations. The numerical model is actually a coupled one consisting of a model for the vehicle and a commercial code model for the soil.

2. Numerical model

The numerical modeling includes two stages:

- Firstly, the dynamic axle load resulting from pavement irregularity is determined using a moving vehicle model composed of springs, dampers and lumped mass. In the case of vehicle–road interaction, several authors indicate that the prediction of the dynamic axle loads can be uncoupled from the solution of the road-soil interaction problem due to the high stiffness of the road compared to the vehicle's suspension system or tyres [14–17]. More recently, the validity of this assumption has been confirmed by the study of Lombaert and Degrande [18] based on the model of a beam on a Winkler foundation for the road. The same assumption is adopted in the present study.
- The resulting axle dynamic load is then used in a 3D numerical modeling for the determination of the ground vibrations due to the load determined in the first stage.

In recent years, several models have been proposed for the determination of the vehicle dynamic axle load due to the road unevenness. These models range from simplified models to more complex MDOF models. Some authors assumed that the axle load could be represented by a half sine wave with a frequency deduced from the time required to load and unload the force during the passage of the vehicle on the contact surface. Watts and Krylov [2] and Cebon [15] used a 2DOF quarter-car model to analyze the interaction between heavy vehicles and roads. Lombaert and Degrande [6,7] used a 4DOF half car model for a two-axle truck. More sophisticated vehicle models, such as the 7DOF model for a tractor–trailer vehicle [19] or the full-scale two-axle vehicle model [20], were used to analyze the bridge dynamic response.

In this paper, a four degree-of-freedom half-car model is used for the determination of the vehicle dynamic response to road irregularities. This model considers the vehicle pitch motions, the body motions and the center of gravity effect. Furthermore, the differences between front and rear dampers and spring characteristics can be modeled properly as depicted in Fig. 1.

The equations of motion for the vehicle body and front and rear wheels can be summarized as follows [21]:

$$[M](\ddot{X}) + [C](\dot{X}) + [K](X) = (P) \tag{1}$$

where

$$[M] = \begin{bmatrix} m_s & 0 & 0 & 0 \\ 0 & I_s & 0 & 0 \\ 0 & 0 & m_{u2} & 0 \\ 0 & 0 & 0 & m_{u1} \end{bmatrix},$$

$$[C] = \begin{bmatrix} c_{s1}+c_{s2} & c_{s2}l_1 + c_{s1}l_2 & -c_{s2} & -c_{s1} \\ c_{s2}l_2 + c_{s1}l_1 & c_{s2}l_2^2 + c_{s1}l_1^2 & -c_{s2}l_2 & -c_{s1}l_1 \\ -c_{s2} & -c_{s2}l_2 & c_{s2} & 0 \\ -c_{s1} & -c_{s1}l_1 & 0 & c_{s1} \end{bmatrix}$$

$$[K] = \begin{bmatrix} k_{s1}+k_{s2} & k_{s2}l_1 + k_{s1}l_2 & -k_{s2} & -k_{s1} \\ k_{s2}l_2 + k_{s1}l_1 & k_{s2}l_2^2 + k_{s1}l_1^2 & -k_{s2}l_2 & -k_{s1}l_1 \\ -k_{s2} & -k_{s2}l_2 & k_{s2}+k_{t2} & 0 \\ -k_{s1} & -k_{s1}l_1 & 0 & k_{s1}+k_{t1} \end{bmatrix},$$

$$(P) = \begin{bmatrix} 0 \\ 0 \\ P_2 \\ P_1 \end{bmatrix}, (X) = \begin{bmatrix} x_s \\ \theta_s \\ x_{u2} \\ x_{u1} \end{bmatrix} \tag{2}$$

Here, m_s, m_{u1} and m_{u2} are the masses of the vehicle body and the front and rear wheels, respectively; I_s denotes for the mass moment of inertia for the vehicle body; c_{s1}, c_{s2}, k_{s1}, and k_{s2} are the damping coefficients and the spring stiffnesses of the front and rear suspension, respectively; k_{t1} and k_{t2} are the front/rear stiffnesses; l_1 and l_2 are shown in Fig. 1 and $l = l_1 + l_2$.

The parameter θ_s is the rotation at the center of gravity and x_s is the vertical displacement of the vehicle body at the center of gravity.

x_s and θ_s are given by the following equations:

$$x_s = (l_2 x_{s1} + l_1 x_{s2})/l \qquad \theta_s = (x_{s1} - x_{s2})/l \tag{3}$$

where $x_{s1/xs2}$ are the vertical displacement of the vehicle body at the front/rear suspension location, and x_{r1} and x_{r2} are the irregularity excitation from the pavement surface at the location of front/rear tire. P_1 and P_2 are the interaction forces between the front and rear axle and the pavement, where

$$P_1(t) = k_{t1}(x_{u1}(t) - x_{r1}(t)) \qquad P_2(t) = k_{t2}(x_{u2}(t) - x_{r2}(t)) \tag{4}$$

Ground vibrations due the axle loads P_1 and P_2 are determined using the FLAC3D program, which is based on a 3D finite difference modeling. The material viscosity is considered using Rayleigh damping for the energy dissipation through the medium [22]. Absorbing elements based on viscous dashpots are used on the

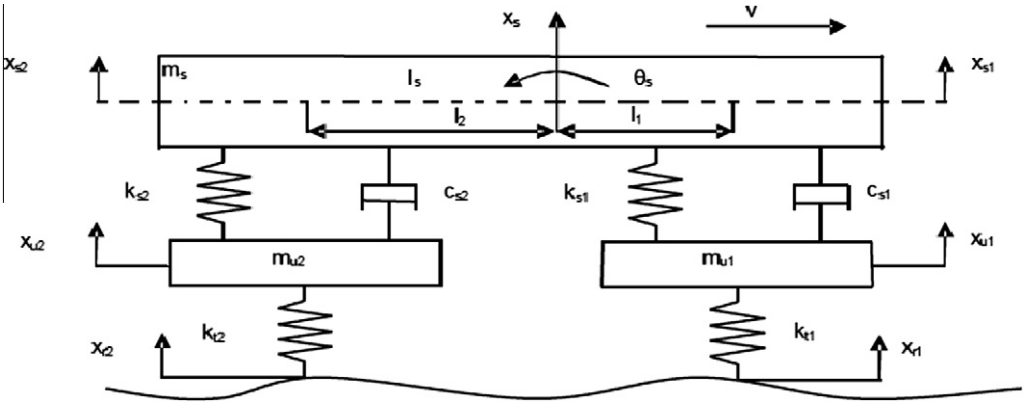

Fig. 1. 4DOF half car model of the vehicle.

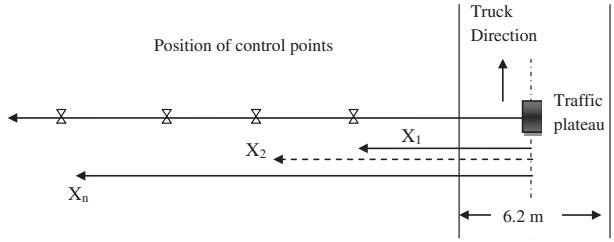

Fig. 2. General road layout used in the experimental study.

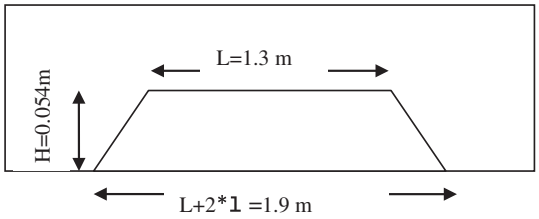

Fig. 3. Longitudinal profile of the road unevenness.

lateral boundaries to reduce wave reflection. These boundaries are provided by Flac3D. Details of these elements are given by Lysmer and Kuhlemeyer [23]. These boundaries are placed at a sufficient distance from the region of interest to minimize the effect of reflected waves.

3. Validation of the numerical model

3.1. Description of the case study

The numerical model is validated using field data from Lombaert and Degrande [7], who measured ground vibrations due to the passage of a Volvo FL6 truck on artificial road unevenness at vehicle speeds between 23 and 58 km/h. Fig. 2 shows the cross section of the road and the control points used in the field measurements.

The road pavement consists of three layers: an asphalt top layer, a crushed stone layer and a crushed concrete layer. Table 1 summarizes the layer characteristics: the layer thickness d, the Poisson ratio v, the Young's modulus E and the density ρ. The subgrade soil layers are mainly composed of loam. Their characteristics are summarized in Table 2.

Two kinds of road unevenness can be distinguished: local road unevenness, which is only present at a limited distance along the road, and global road unevenness, which corresponds to the overall unevenness along the road. In the present survey, the artificial unevenness is taken as a traffic plateau with two ramps and a flat midsection, as illustrated in Fig. 3. The unevenness height is equal to $H = 0.054$ m, two slopes of length $l = 0.3$ m and a flat top part with a length $L = 1.3$ m.

3.2. Axle load

The axle load is calculated using Eq. (1). The car parameters are summarized in Table 3. The road unevenness profile is expressed in the time domain in terms of the vehicle speed. Eigen analysis gives the Eigen modes of the truck, 10.8 and 12.4 Hz, which correspond to the front and rear axle hop, and 1.9 and 1.4 Hz, which correspond to the body bounce and pitch of the front and rear axle, respectively.

Fig. 4 displays the front axle load of the truck for two vehicle speeds, $V = 30$ and 58 km/h. The results are in good agreement with those obtained by the frequency response functions (FRF) [7].

Table 1
Characteristics of the road pavement layers.

Layer type	D (m)	v	ρ (kg/m^3)	E (MPa)
Asphalt	0.15	0.33	2100	9150
Crushed stone	0.2	0.45	2000	500
Crushed concrete	0.25	0.45	1800	200

Table 2
Characteristics of the subgrade soil layers.

Layer	D (m)	v	ρ (kg/m^3)	E (MPa)
1	0.5	0.33	1900	57
2	0.5	0.33	1900	133
3	1.5	0.33	1900	223
4	6	0.47	2000	322
5	∞	0.47	2000	1288

Table 3
Parameters of the vehicle [7].

$m_s = 9000$ kg	$k_{s1} = 0.32 \times 10^6$ N/m	$c_{s1} = 10{,}050$ N s/m
$I_s = 35{,}000$ kg/m^2	$k_{s2} = 0.61 \times 10^6$ N/m	$c_{s2} = 16{,}000$ N s/m
$m_{u1} = 400$ kg	$k_{t1} = 1.5 \times 10^6$ N/m	$l_1 = 3.72$
$m_{u2} = 600$ kg	$k_{t2} = 3 \times 10^6$ N/m	$l_2 = 1.49$

3.3. Finite difference modeling

3.3.1. Model description and axle load implementation

The finite difference mesh used in the numerical modeling is illustrated in Fig. 5. It includes 53,130 8-node elements. The size of the model is $30 \times 21 \times 15$ m^3 (length/width/depth). The mesh is refined in the vicinity of pavement layer where the element size is $0.3 \times 0.3 \times 0.15$ and increases gradually when approaching boundaries along the x and z axes. Due to the symmetry of both the geometry and loading, half of the domain is considered.

Calculations are performed with the following boundary conditions:

- The base of the soil mass is assumed to be rigid.
- The x displacements are fixed along the symmetry plane y–z.
- Viscous dashpots are used at lateral boundaries.

A Matlab subroutine is developed to automatically apply the axle load on the finite difference model. The vehicle path at the pavement surface is discretized by square elements (0.3 m^2) that correspond to the wheel footprint. The axle load is applied on the path elements as a pressure deduced from the time-domain axle load and the vehicle speed as follows:

- The passage time over an element of a size Δx (0.3 m in our case) for a vehicle speed V is $\Delta T = \Delta x/V$.
- The axle load is divided in the time domain into L intervals of width equal to ΔT.

The axle load is discretized using a time step $\Delta t = 0.0005$ s. This time step is adequate to correctly reproduce the load movement. For example, for a vehicle speed of $V = 60$ km/h, the time required to pass over an element of 0.3 m is approximately $\Delta T = 0.018$ s, so the applied pressure is represented by $n = \Delta T/\Delta t = 36$ points for each element.

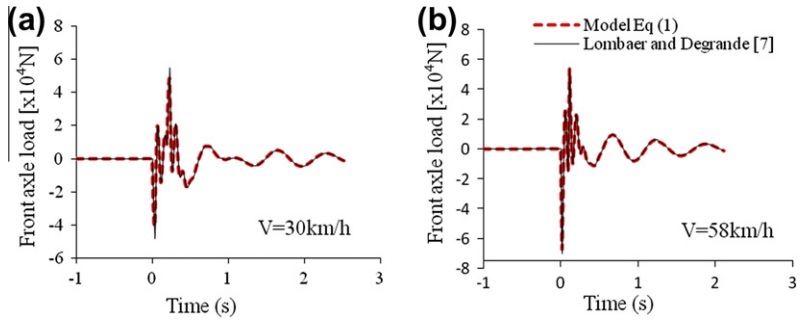

Fig. 4. Time history of the front axle load for the passage of the vehicle on the road unevenness at a vehicle speed (a) $V = 30$ km/h, (b) $V = 58$ km/h.

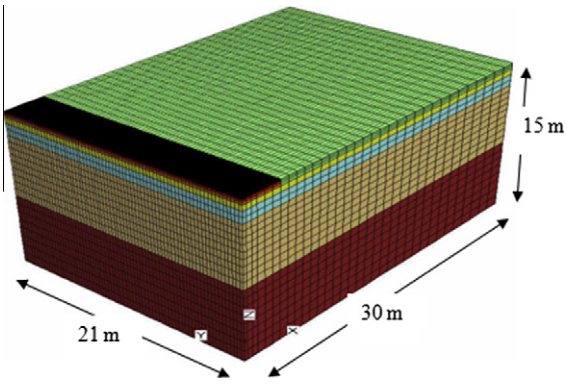

Fig. 5. 3D numerical mesh with adsorbing viscous boundaries (57,936 nodes, 53,130 elements) pavement and subgrade soil layers (see Tables 1 and 2).

3.3.2. Numerical results

Figs. 6 and 7 show a comparison of the predicted velocities using the numerical model and the field data reported in [7] for a vehicle speed of $V = 30$ km/h. Both the vertical and transverse particle velocities (V_z and V_x) are compared at distances of $X = 8$ m and 16 m from the load axis. The horizontal vibration V_y is relatively small and is ignored in this study.

A good agreement is observed between the numerical results and the field data. Results in the vertical direction V_z are of the same order of magnitude for $X = 8$ m and $X = 16$ m. In the transverse direction, the numerical model gives acceptable results at $X = 8$ m but underestimates the velocity at $X = 16$ m.

The velocity time history includes two parts. The first one corresponds to the passage of the first axle on the traffic plateau, and the second corresponds to the passage of the second axle. For each part, two principal peaks are observed; they correspond

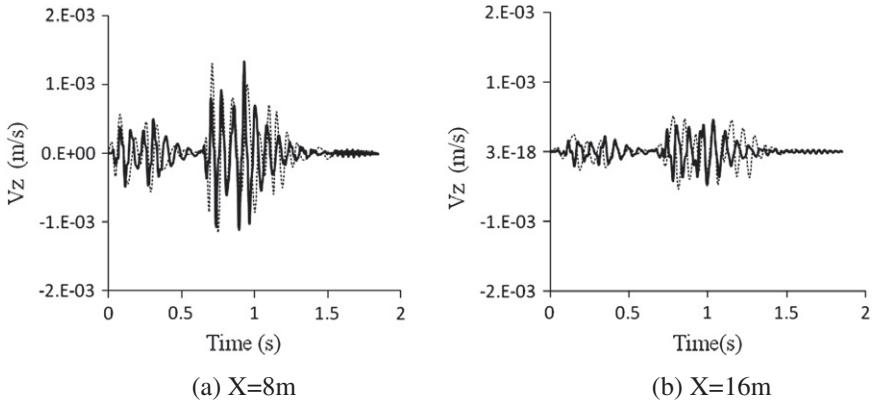

Fig. 6. Time history of measured and predicted free field vertical particle velocity V_z – Vehicle speed $V = 30$ km/h (predicted: solid line; measured: dashed line).

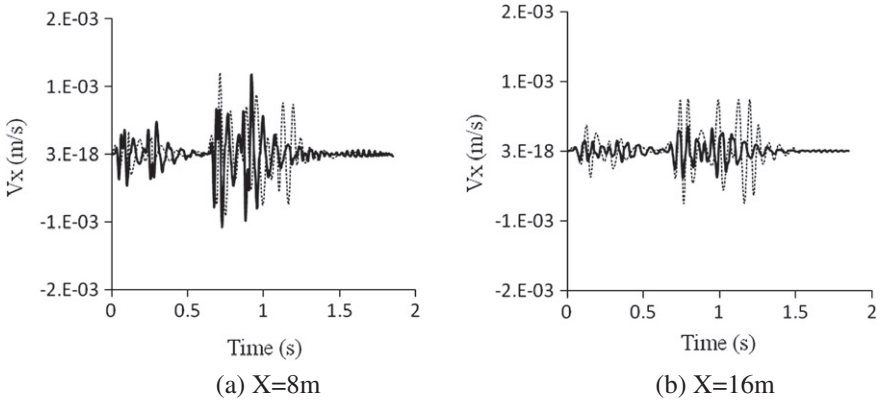

Fig. 7. Time history of measured and predicted free field transverse particle velocity V_x – Vehicle speed $V = 30$ km/h (predicted: solid line; measured: dashed line).

Table 4
Influence of the vehicle speed on the ground vibrations (V_z in mm/s).

Vehicle speed (km/h)	Distance from the road center (m)					
	4	8	12	16	20	24
15	0.57	0.322	0.22	0.16	0.116	0.114
30	2.361	1.335	0.812	0.485	0.459	0.437
45	3.07	1.44	0.9	0.75	0.605	0.519
60	3.78	1.925	1.467	1.24	1.14	0.86

to phases of the mounting and descent of the traffic plateau, respectively. The time interval between the two parts corresponds well to the time required for the second axle to reach the traffic plateau.

4. Parametric analysis

This section presents a parametric analysis of the influence on ground vibrations of key parameters such as the vehicle speed, the type of speed cushions generally used in France and the suspension system. Analyses are conducted with the data from the validation example.

4.1. Influence of the vehicle speed

Table 4 and Fig. 8 show the influence of the vehicle speed V on the induced ground vibrations. The vehicle speed greatly affects the ground vibrations. The attenuation of the peak particle velocity V_z (resp. V_x) due to the radiation and material damping is illustrated in Fig 8a (resp. Fig. 8b). This attenuation could be expressed as follows:

$$Ln(V_z/V) = aX + b \tag{5}$$

X denotes the distance from road center, and a and b are constants dependent on the road unevenness configuration and the soil characteristics. A similar formula could be derived for the vibration V_x.

4.2. Influence of the surface unevenness

Analyses were conducted with a vehicle speed $V = 36$ km/h for three types of speed reducers (Fig. 9). They correspond to the

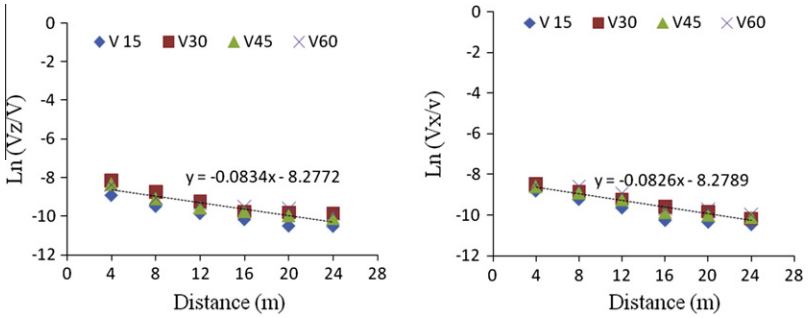

Fig. 8. Influence of vehicle speed on the free field particle velocity in both (a) transversal and (b) vertical directions.

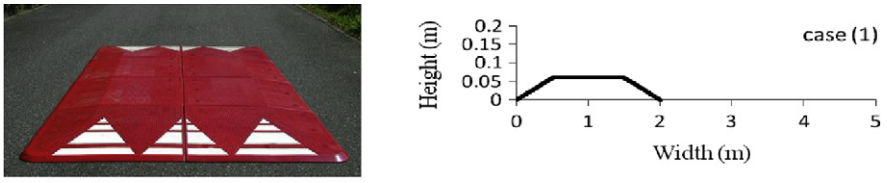

(a) Speed Cushion (Case 1)

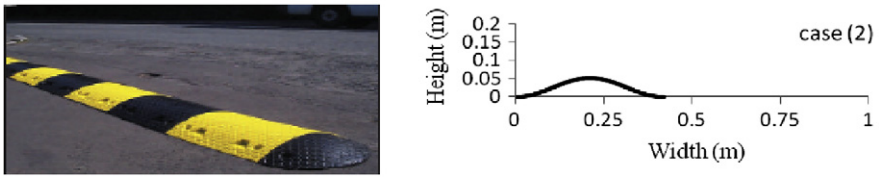

(b) Short hump (Case 2)

(c) Trapezoidal traffic calming (Case 3)

Fig. 9. Different profiles of speed reducers used in the numerical model.

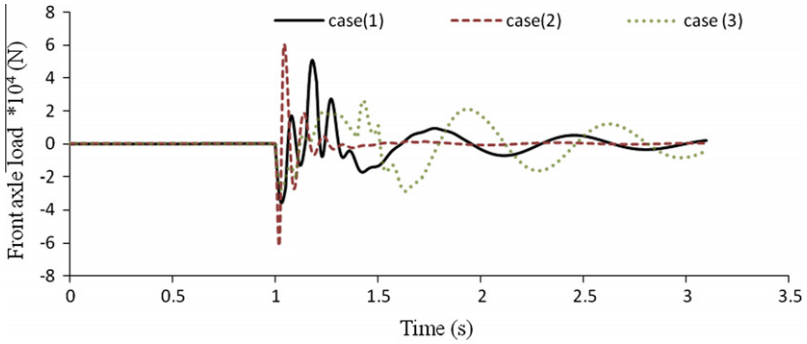

Fig. 10. Time history of the front axle load induced by different speed reducers – V = 36 km/h.

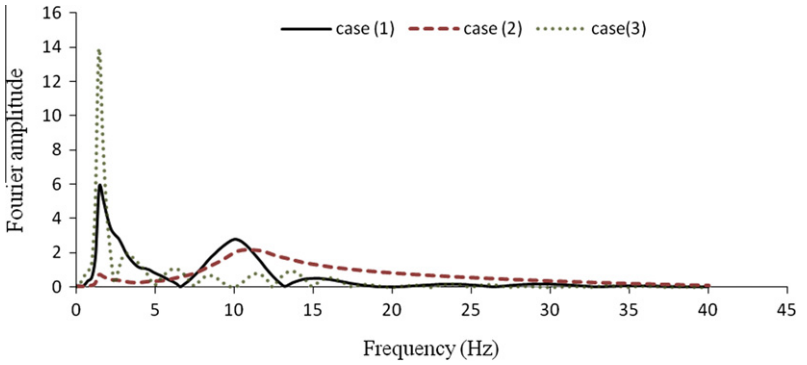

Fig. 11. Frequency content of the front axle load induced by different speed reducers – V = 36 km/h.

Table 5
Influence of the speed reducer geometry on the ground vibrations (V_z in mm/s)(V = 36 km/h).

Case	Distance from the road center (m)					
	4	8	12	16	20	24
(1)	1.45	0.57	0.42	0.36	0.29	0.19
(2)	6.48	2.46	2.08	1.97	1.52	0.93
(3)	1.02	0.43	0.28	0.18	0.15	0.13

Table 6
Influence of the speed reducer geometry on the ground vibrations (V_x in mm/s) (V = 36 km/h).

Case	Distance from the road center (m)					
	4	8	12	16	20	24
(1)	1.25	0.76	0.49	0.31	0.26	0.21
(2)	4.82	4.27	3.06	1.41	1.23	0.85
(3)	0.69	0.43	0.28	0.16	0.13	0.12

French regulations given by the center for studies on urban planning, transportation and public facilities [24]. The speed cushion (case 1) has a total length of 2 m and a height of 0.06 m; it includes two ramps of 0.5 m. The short hump (case 2) has a sinusoidal shape that is 420 mm in width and 50 mm in height. The wide trapezoidal traffic calming (case 3) has a flat top part of 3 m and two ramps of 1 m in length.

Fig. 10 shows the front axle load induced by the passage of the vehicle on different speed reducers. The short hump (case 2) induces the highest load. Fig. 11 shows the frequency content of the front axle load. For the speed reducers 1 and 3, the dominant frequency is close to 2 Hz, which corresponds to the pitch and bounce mode, while the dominant frequency of speed reducer 2 is close to 10 Hz, which corresponds to the axle hop mode. In all cases, the frequency content is mainly situated below 20 Hz. This result agrees well with measurements realized in [4].

Table 7
Characteristics of the suspension systems.

Suspension type	Vertical stiffness (N/m)	Damping coefficient (N s/m)
Air suspension	0.4e6	10,000
Leaf spring	2e6	10,000

Table 8
Influence of the suspension system on the ground vibrations (V_z mm/s) V = 36 km/h (Case 2).

Type of suspension	Distance (m)					
	4	8	12	16	20	24
Air suspension	6.87	2.85	2.36	2.12	1.625	1.09
Leaf springs	6.38	2.53	2.00	1.87	1.43	0.97

Tables 5 and 6 summarize the influence of the speed reducer on the ground vibrations induced by the vehicle passage. The short hump (case 2) produces the highest response despite its lower height. Furthermore, the ground vibration in this case exceeds the threshold of vibrations allowed in urban areas. This result meets the recommendation of the UK Department of Transport, which limits the height of humps used as a traffic-calming measure in proximity to buildings to 40 mm [25].

The comparison between the speed cushion (case 1) and the trapezoidal traffic calming (case 3) shows that the ramp slope largely affects the ground vibration. The vibration level of the 1st case is higher than that of the 3rd case despite the greater height of the

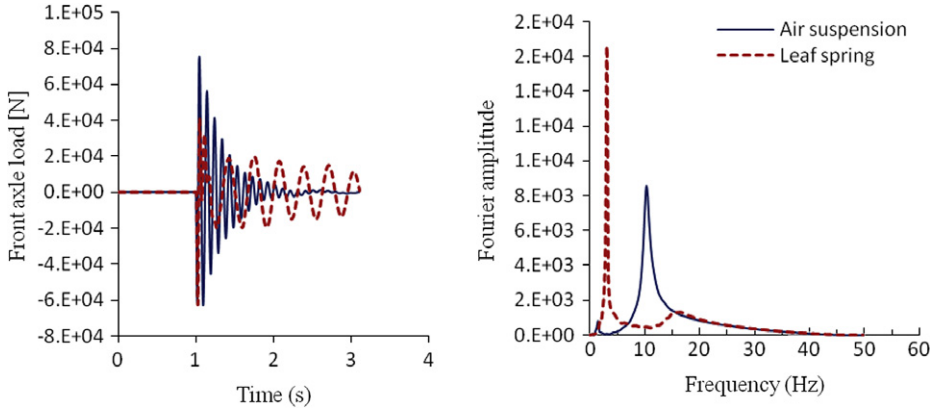

Fig. 12. Influence of suspension system on the front axle load.

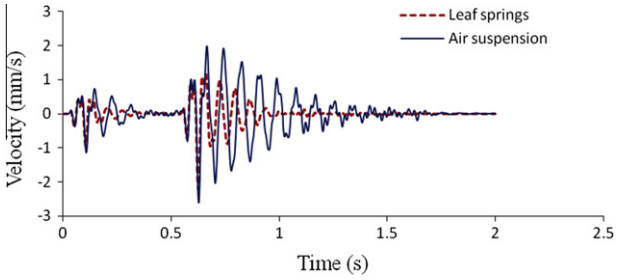

Fig. 13. Influence of the suspension system on the particle velocity at $X = 10$ m from the road center.

latter. The slope of the first case is equal to 12%, to be compared with that of the 3rd case (10%). In Belgium, a slope of 5% is imposed for road humps used by buses and heavy traffic [26].

4.3. Influence of the suspension system

Experimental tests conducted by Hunaidi and Rainer [27] showed that the modification in the heavy vehicle suspension could significantly reduce the traffic-induced vibrations. The suspension of a heavy vehicle affects both the amplitude of the axle load and the axle hop frequency. It mainly depends on the suspension vertical stiffness and suspension damping. The spring stiffness is generally designed to be adjustable with the applied load. Leaf spring and air suspensions are widely used. The leaf spring relies on the Coulomb friction, while the air suspension relies on the shock absorbers. In addition, the spring rate in the air suspension system is highly dependent on the rate loading, which is not the case in the leaf spring suspension system.

Table 7 gives the characteristics of the suspension systems used in the analysis. They were selected according to typical suspensions proposed in literature [28,29].

Fig. 12a displays the front axle load due to the vehicle passage at a speed of $V = 36$ km/h over the short hump (case 2). Fig. 12b shows the influence of the suspension system on the dominant frequency of the axle load. For the leaf spring system, the dominant frequency (2 Hz) corresponds to a bounce and pitch mode, while the hop axle mode is dominant for the air suspension system. Table 8 summarizes the results of the analysis on the ground vibrations. The use of the leaf spring suspension leads to a reduction of about 10–20% in the vibration levels in comparison with the air suspension system. Fig. 13 shows a rapid attenuation in the ground vibration obtained with the leaf spring system, even for a relatively large and long continuation of the front axle load with low frequency (2 Hz).

5. Conclusion

This paper presented a numerical model for the analysis of the ground vibrations resulting from road traffic. A car model with 4DOF was used to determine the load due to the road irregularity. A 3D finite difference model was then used for the determination of the traffic-induced ground vibrations. The validation of numerical model on field data gave satisfactory results and showed the capacity of the proposed model to reproduce the ground vibrations resulting from the road traffic.

Analyses showed that both the amplitude and frequency of the traffic-induced ground vibrations were affected by the vehicle speed, the geometry of the speed reducer and the vehicle suspension system. On the basis of the numerical results, short humps should be avoided, and preferences should be given to the leaf spring vehicle suspension system.

The numerical model can be used for analysis of the traffic-induced ground vibration in the presence of superstructures or barriers. It is also useful for the analysis of technologies proposed for the reduction of both the traffic-induced vibrations and their impact on the environment.

References

[1] Watts GR, Harris GJ, Layfield RE. Traffic calming, vehicle generated groundborne vibration alongside speed control cushions and road humps. Transport research laboratory, TRL report 235; 1997.
[2] Watts GR, Krylov VV. Ground-borne vibration generated by vehicles crossing road humps and speed control cushions. J Appl Acoust 2000;59(3):221–36.
[3] Crispino M, D'Apuzzo M. Measurement and prediction of traffic-induced vibrations in a heritage building. J Sound Vib 2001;246(2):319–35.
[4] Hunaidi O, Guan W, Nicks J. Building vibrations and dynamic pavement loads induced by transit buses. J Soil Dyn Earthq Eng 2000;19(6):435–53.
[5] Hunaidi O, Tremblay M. Traffic-induced building vibrations in Montréal. Can J Civil Eng 1997;24(5):736–53.
[6] Lombaert G, Degrande G. Experimental validation of a numerical prediction model for free field traffic induced vibrations by in situ experiments. J Soil Dynam Earthq Eng 2001;21(6):485–97.
[7] Lombaert G, Degrande G. The experimental validation of a numerical model for the prediction of the vibrations in the free field produced by road traffic. J Sound Vib 2003;262(2):309–31.
[8] D'Apuzzo M. Some remarks on the prediction of road traffic induced groundborne vibrations. In: 4th international SIIV congress, Palermo, Italy; 2007.
[9] Shen HJ. Finite element investigation of traffic induced vibrations. J Sound Vib 2009;321(3–5):837–53.
[10] Xu YL, Hong XJ. Stochastic modeling of traffic-induced building vibration. J Sound Vibr 2008;313(1–2):149–70.
[11] Cao YM, Xia H, Lombaert G. Solution of moving-load-induced soil vibrations based on the Betti–Rayleigh dynamic reciprocal theorem. J Soil Dynam Earthq Eng 2010;30(6):470–80.

[12] Hajek J, Blaney CT, Hein DK. Mitigation of highway traffic induced vibration. Annual Conference of the Transportation Association of Canada. Charlottetown Prince Edward Island; 2006.
[13] Beskou ND, Theodorakopoulos DD. Dynamic effects of moving loads on road pavements: a review. J Soil Dynam Earthq Eng 2011;31(4):547–67.
[14] Markow MJ. Analyzing the interaction between dynamic vehicle loads and highway pavements. Transport Res Rec TRB 1988;1196:161–9.
[15] Cebon D. Interaction between heavy vehicles and roads. Society of Automotive Engineers; 1993. ISBN 1-56091-336-3.
[16] Gillespie TD, Karamihas SM, Sayers MW, Nasim MA, Hansen W, Ehsan N. Effects of heavy-vehicle characteristics on pavement response and performance. Technical Report 353, NCHRP, Transportation Research Board, Washington DC; 1993.
[17] Mamlouk MS. General outlook of pavement and vehicle dynamics. J Transport Eng, Proc ASCE 1997;123(6):515–7.
[18] Lombaert G, Degrande G. Study of determining factors for traffic induced vibrations in buildings. First biannual report BWM-1999-01, Department of Civil Engineering, Katholieke Universiteit Leuven, January 1999. DWTC Research Programme Sustainable Mobility, Research Project MD/01/040; 1999.
[19] Law SS, Zhu XQ. Bridge dynamic responses due to road surface roughness and braking of vehicle. J Sound Vib 2005;282(3–5):805–30.
[20] Deng L, Cai CS. Identification of parameters of vehicles moving on bridges. J Eng Struct 2009;31(10):2474–85.
[21] Law SS, Bu JQ, Zhu XQ, Chan SL. Vehicle axle loads identification using finite element method. J Eng Struct 2004;26(8):1143–53.
[22] Lokmer I, Herak M, Panza GF, Vaccari F. Amplification of strong ground motion in the city of Zagreb, Croatia, estimated by computation of synthetic seismograms. J Soil Dynam Earthq Eng 2002;22(2):105–13.
[23] Lysmer J, Kuhlemeyer RL. Finite dynamic model for infinite media. J Eng Mech 1969;95:859–77. EM4.
[24] CERTU. Centre d'études sur les réseaux, les transports, l'urbanisme et les constructions. Guide les ralentisseurs de type dos d'âne et trapézoïdale textes et recommandations; 1994.
[25] Traffic Advisory Leaflet 8/96. Road humps and ground-borne vibration, Department for Transport in England; 1996.
[26] Lombaert G. Development and experimental validation of a numerical model for the free field vibrations induced by road traffic. Ph.D. Thesis, Catholic university of Leuven., Belgium; 2001.
[27] Hunaidi O, Rainer JH. Control of traffic-induced vibration in buildings using vehicle suspension systems. J Soil Dynam Earthq Eng 1996;15(4):245–54.
[28] Fu T, Cebon D. Analysis of a truck suspension database. J Veh Des, Heavy Veh Syst 2002;9(4):281–97.
[29] Douglas WH, Darren JT, Karen RR. Review of truck characteristics as factors in roadway design. Report 505, transportation research board Washington, DC; 2003